Available online at www.sciencedirect.com

ScienceDirect

Ceramics International 40 (2014) 4725–4730

CERAMICS INTERNATIONAL

www.elsevier.com/locate/ceramint

Effect of Eu^{3+} concentration on the luminescence properties of $Y_2O_2S:Eu^{3+}$, Mg^{2+}, Ti^{4+} nanotubes

Cai'e Cui[a,b], Guowei Jiang[a], Ping Huang[a,*], Lei Wang[a], Dan Liu[a]

[a]*Physics and Optoelectronic Engineering College, Taiyuan University of Technology, Taiyuan 030024, China*
[b]*Observation and Control Technology Research Institute, Taiyuan University of Technology, Taiyuan 030024, China*

Received 11 July 2013; received in revised form 27 August 2013; accepted 4 September 2013
Available online 12 September 2013

Abstract

Red long-lasting phosphor $Y_2O_2S:Eu^{3+}$, Mg^{2+}, Ti^{4+} nanotubes were synthetized by the hydrothermal method. The effect of Eu^{3+} doping concentration on the luminescence properties was investigated. The samples were examined using X-ray diffraction (XRD), scanning electron microscopy (SEM), photoluminescence (PL) and thermoluminescence spectra (TL). The results of XRD revealed that the precursors were a pure phase of $Y(OH)_3$ and the sulfuretted samples were a pure phase Y_2O_2S. SEM observation showed that the phosphors with diameters of 200–400 nm and lengths of 2–3 μm inherited the tube-like shape from the precursor after calcination in CS_2 atmosphere. Under 325 nm UV excitation, the emission peaks at 625 nm were assigned to the $^5D_0 \rightarrow {}^7F_2$ transition of Eu^{3+}. When the content of Eu^{3+} dopant was 5.0%, the trap depth of sample was 0.88 eV and the decay time could last for over 1175 s (≥ 1 mcd/m^2) after 365 nm UV radiation for 10 min.

Keywords: Red long-lasting phosphor; $Y_2O_2S:Eu^{3+}$, Mg^{2+}, Ti^{4+}; Nanotubes; Luminescence

1. Introduction

Long-lasting phosphors which can still light up for a long time after removal of the excitation source are one of photoluminescent materials. Due to the unique property, long-lasting phosphors are widely applied to several fields such as emergency lighting, road signs, optical mark and safety indication [1–6]. The luminescence properties of long-lasting phosphors are greatly affected by the particle size, morphology, surface structure and crystalline state. When the grain size reaches to nano-scale, some new properties will be obtained as a result of both their specific shape and quantum-confinement structure [7]. In recent years, preparation and properties of the one-dimensional nanometer luminescent materials have attracted much attention of research groups. Up to now, much work has been done in this field. During the research, some methods have been proposed for the preparation of fine powders in nano-size, including sol–gel method [8], chemical precipitation [9], solid phase method [10], hydrothermal synthesis [11] and so on. The hydrothermal method which has advantages of low processing temperature, high homogeneity and purity of the products has become a promising method for the preparation of well-crystallized nanomaterials. A great many nanocrystal phosphors with controlled morphology have been synthesized, such as some rare earth oxides and hydroxides, Y_2O_3, Eu_2O_3, $Y(OH)_3$, $Eu(OH)_3$, $La(OH)_3$, $Gd(OH)_3$ and so on [12–15]. As for rare earth oxysulfide materials, Y_2O_2S, Gd_2O_2S, Eu_2O_2S and La_2O_2S are known as nanorods [7], La_2O_2S and Nd_2O_2S as nanowires [16] and Y_2O_2S as nanotubes [12].

Eu^{3+}-doped oxysulfides were widely studied as efficient red emitting phosphors due to the abundant transitions from the excited $^5D_0$ level to the ^7F_J ($J=0$, 1, 2, 3, and 4) levels of the $4f^6$ configuration in the orange–red light area [17–19]. The long-lasting phosphor $Y_2O_2S:Eu^{3+}$, Mg^{2+}, Ti^{4+} has been known as the best red luminescent material at present. In Y_2O_2S host, Eu^{3+} substitutes the site of Y^{3+}, and as the luminescence center, it plays a decisive role in the luminescence properties of $Y_2O_2S:Eu^{3+}$, Mg^{2+}, Ti^{4+} nanotubes. In the past, $Y_2O_2S:Eu^{3+}$, Mg^{2+}, Ti^{4+} nanotubes were synthetized by the hydrothermal method, the nanotubes $Y_2O_2S:Eu^{3+}$, Mg^{2+}, Ti^{4+} phosphor have promising long-lasting phosphorescence and uniform size. In a previous work,

*Corresponding author. Tel.: +86 0351 4175345.
E-mail address: huangpinghuangka@163.com (P. Huang).

0272-8842/$ - see front matter © 2013 Elsevier Ltd and Techna Group S.r.l. All rights reserved.
http://dx.doi.org/10.1016/j.ceramint.2013.09.015

the effects of simultaneous change of Mg^{2+} and Ti^{4+} contents on the luminescence properties of $Y_2O_2S:Eu^{3+}$, Mg^{2+}, Ti^{4+} nanotubes were investigated [20]. However, the effect of Eu^{3+} concentrations on $Y_2O_2S:Eu^{3+}$, Mg^{2+}, Ti^{4+} phosphors prepared using hydrothermal method is still unknown and is needed to be investigated.

In this paper, the precursor $Y(OH)_3:Eu^{3+}$, Mg^{2+}, Ti^{4+} nanotubes have been prepared via the hydrothermal method. Then the precursor has been sulfuretted in CS_2 atmosphere to obtain the long afterglow phosphor $Y_2O_2S:Eu^{3+}$, Mg^{2+}, Ti^{4+}. The effect of Eu^{3+} doping concentration on the crystal characteristics, morphology, luminescence properties and afterglow performance of $Y_2O_2S:Eu^{3+}$, Mg^{2+}, Ti^{4+} phosphors are discussed.

2. Experiment

Y_2O_3 (3N), $Eu(NO_3)_3 \cdot 6H_2O$ (4N), $Mg(NO_3)_2 \cdot 6H_2O$ (99.0%), $C_{16}H_{36}O_4Ti$ (98%), NaOH ($>96\%$), HNO_3 ($65\sim68\%$), C_2H_5OH ($>99.7\%$), S (99.5%) and C (99.0%) were employed as the starting materials. Rare-earth nitrate stock solutions were prepared by dissolving the corresponding metal oxide in nitric acid at elevated temperatures. A tube-like $Y(OH)_3$ precursor, co-doped with Eu, Mg and Ti, was prepared by the hydrothermal method. In a typical procedure, 10 ml $Y(NO_3)$ (0.5 M), 5 ml $Eu(NO_3)_3$ (0.05 M), 3 ml $Mg(NO_3)_2$ (0.05 M), 3 ml $C_{16}H_{36}O_4Ti$ (0.05 M) were mixed to get a component with $Y^{3+}:Eu^{3+}:Mg^{2+}:Ti=100:5:3:3$ in mole ratio. Then 14 ml H_2O and 7 ml ethanol were added into the well-prepared materials. The as-obtained solution's pH was adjusted to 13 using NaOH (4 M), and stirred for 2 h at room temperature. Afterwards the solution was poured into the teflonlined autoclave and the filling volume of the solution was 80% of the reactor. Teflonlined autoclaves were heated at 180 °C for 12 h. After naturally cooling to room-temperature, the precursors were separated by filtration, washed with deionized water, and dried in the air at 60 °C overnight. To investigate the effect of Eu^{3+} doping concentration on the luminescence properties, we defined the content of Eu^{3+} dopant as X ($X=1.0$, 2.0, 3.0, 4.0, 5.0 and 6.0 mol%). $Y(OH)_3:Mg^{2+}$, Ti^{4+} precursors with different X doping were systematically prepared in a similar way. Then these precursors were calcined at 750 °C for 6 h in CS_2 atmosphere which was formed by the reaction of sulfur and carbon. Finally, the precursors formed the tube-like long afterglow phosphors $Y_2O_2S:Eu^{3+}$, Mg^{2+}, Ti^{4+}.

X-ray powder diffraction (XRD) was used to check the phase of the samples at 40 kV and 30 mA using a SHIMADZU-6000 X-ray generator with Cu Kα ($\lambda=0.15406$ nm) radiation and the scan step is 0.02°. The size and morphology of the samples were inspected by a scanning electron microscope (SEM, Hitachi S-4800). Excitation and emission spectra of the powder samples were measured with an F-280 fluorescence spectrophotometer which uses a 150 W Xe lamp as excitation source. The afterglow decay curves were measured with the use of a brightness meter (ST-86LA) with the help of stopwatch. TL spectra of samples were measured on a model FJ-427A1TL meter with a heating rate of 1 K/s from room temperature to 673 K. The samples were excited for 10 min by 365 nm UV radiation standard lamp with a power of 6 W before measuring their TL curves and the afterglow properties. All measurements were carried out at room temperature except for the TL curves.

3. Results and discussion

3.1. Phase characterization

X-ray diffraction is adopted to check the purity of samples. Fig. 1a shows XRD patterns of $Y(OH)_3:Eu^{3+}$, Mg^{2+}, Ti^{4+}

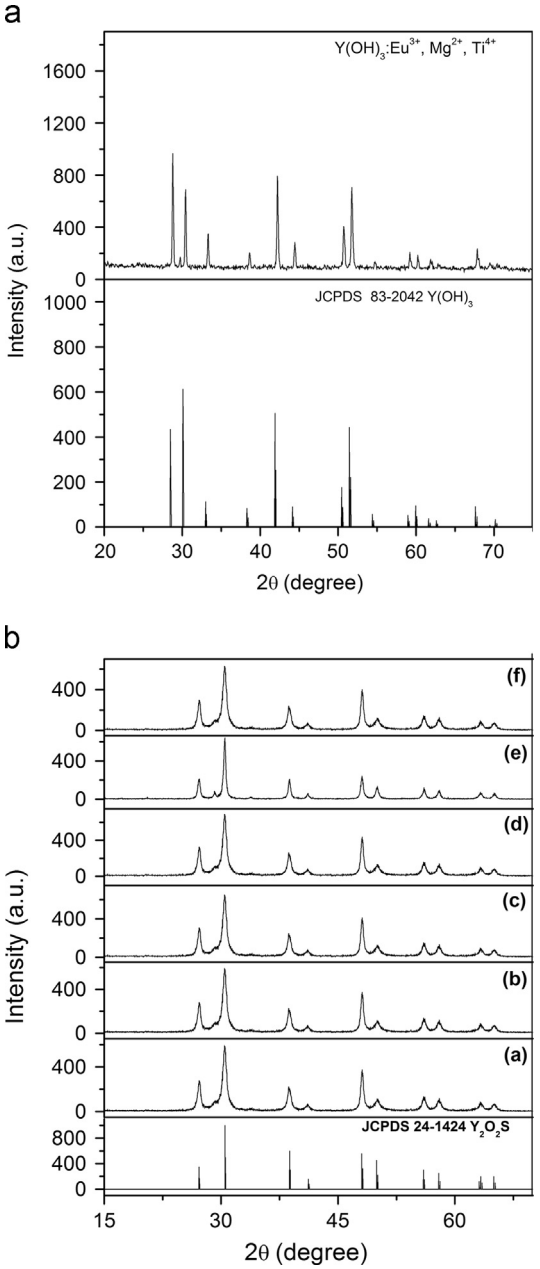

Fig. 1. a XRD patterns of $Y(OH)_3:Eu^{3+}$, Mg^{2+}, Ti^{4+} with X for 5.0 mol%. b XRD patterns of $Y_2O_2S:Eu^{3+}$, Mg^{2+}, Ti^{4+} with different X: (a) 1.0 mol%; (b) 2.0 mol%; (c) 3.0 mol%; (d) 4.0 mol%; (e) 5.0 mol%; (f) 6.0 mol%.

precursor with X for 5.0 mol%. All peaks primly match the values in the standard $Y(OH)_3$ card (PDF #83-2042), and no impurity is detected. Fig. 1b shows XRD patterns of Y_2O_2S:Eu^{3+}, Mg^{2+}, Ti^{4+} with different concentrations of Eu^{3+}. All peaks are in good agreement with the diffraction from hexagonal Y_2O_2S structure, which are very close to the standard lattice parameters provided by the powder diffraction file, PDF #24-1424. The radius of Eu^{3+} (0.112 nm) is close to that of Y^{3+} (0.106 nm), which is just the reason why Eu^{3+} is able to replace the position of Y^{3+} and enters the lattice. Even though Eu^{3+} ions occupy the position of Y^{3+} ions, the development and growth of the Y_2O_2S crystals have not been changed as significantly as the presence of Eu^{3+} ions.

3.2. Morphology of $Y(OH)_3$:Eu^{3+}, Mg^{2+}, Ti^{4+} precursors and Y_2O_2S:Eu^{3+}, Mg^{2+}, Ti^{4+} phosphors

Fig. 2a presents the SEM image of the $Y(OH)_3$:Eu^{3+}, Mg^{2+}, Ti^{4+} with X for 5 mol%. SEM image reveals that samples are open and nanotube-shaped. The precursor with uniform size and good distribution is obtained by the hydrothermal method. The SEM image shows that the outer diameter of precursor is 120–200 nm and the lengths range from 1 to 2 μm. Fig. 2b shows that the SEM image of the Y_2O_2S:Eu^{3+}, Mg^{2+}, Ti^{4+} with X for 5 mol%. It can be clearly seen that the morphologies of Y_2O_2S:Eu^{3+}, Mg^{2+}, Ti^{4+} nanotubes are almost similar to the initial $Y(OH)_3$:Eu^{3+}, Mg^{2+}, Ti^{4+} precursors, implying that the tube-like shape is kept after calcining for 6 h at 750 °C in CS_2 atmosphere. In comparison with the works of Liu et al. [21], in their method, the shape of samples becomes nanoparticles at 700 °C, however, we can keep the nanotube at 750 °C. The reason is that in our method the Eu^{3+}, Mg^{2+} and Ti^{4+} ions are co-doped in $Y(OH)_3$ in the hydrothermal process and avoid the alkali carbonates and sulfur powder melt during the calcination, which thereafter serves as flux and causes the breakdown of the tube-like structure.

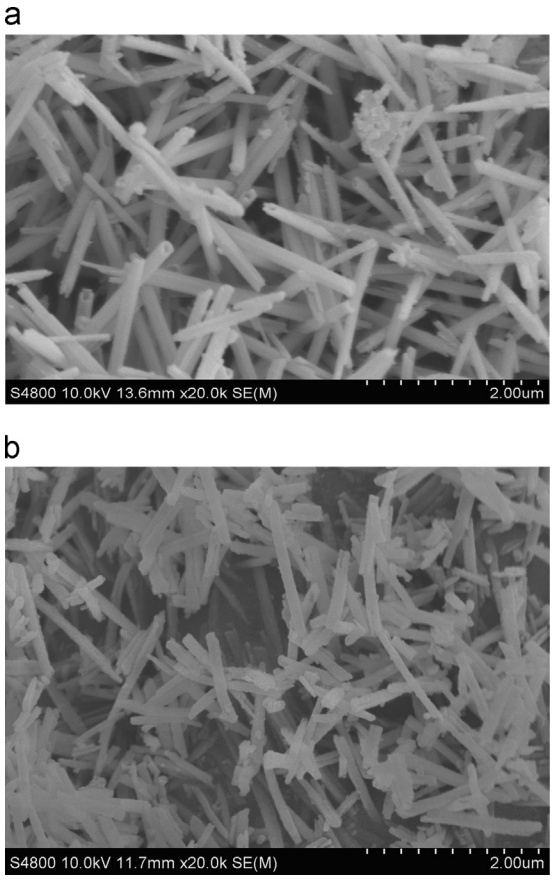

Fig. 2. SEM image of (a) $Y(OH)_3$:Eu^{3+}, Mg^{2+}, Ti^{4+} and (b) Y_2O_2S:Eu^{3+}, Mg^{2+}, Ti^{4+}.

3.3. Luminescence properties of the Y_2O_2S:Eu^{3+}, Mg^{2+}, Ti^{4+} nanotubes

Fig. 3 indicates the excitation spectra of Y_2O_2S:Eu^{3+}, Mg^{2+}, Ti^{4+} nanotubes with different Eu^{3+} dopant contents (X=1.0, 2.0, 3.0, 4.0, 5.0 and 6.0 mol%). It mainly consists of a wide band with two peaks locating near 260 nm and 325 nm as a result of O^{2-}–Eu^{3+} CTB and S^{2-}–Eu^{3+} CTB, respectively. The narrow peaks at 397 nm, 469 nm and 540 nm are attributed to the f–f transition of Eu^{3+} ions [22].

Fig. 4 indicates the emission spectra of Y_2O_2S:Eu^{3+}, Mg^{2+}, Ti^{4+} nanotubes with different Eu^{3+} dopant contents (X=1.0, 2.0, 3.0, 4.0, 5.0 and 6.0 mol%). When the samples are excited under 325 nm UV light, all of spectral lines are in agreement with the intrinsic emission of Eu^{3+}. The strong red-emission lines at 616 nm and 625 nm arise from $^5D_0$ to $^7F_2$ transition of Eu^{3+} while the weaker emission at shorter wavelength values are ascribed to $^5D_1$, $^5D_2$ to ^7F_J (J=0, 1, 2, 3, and 4) transition of Eu^{3+} [23]. The result shows that the samples doped with Mg^{2+} and Ti^{4+} ions do not change the position of emission peaks of Eu^{3+}.

It is known that the luminescence intensity of phosphors is always dependent on the doping concentrations. According to the fluorescence spectra, when the Y_2O_2S:Eu^{3+}, Mg^{2+}, Ti^{4+} phosphor is doped with 5.0 mol% of Eu^{3+}, the intensity of excitation spectra and emission spectra observed reaches the

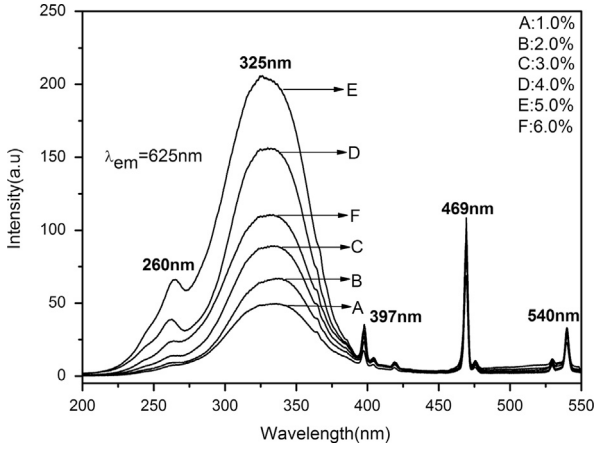

Fig. 3. The excitation spectrums of Y_2O_2S:Eu^{3+}, Mg^{2+}, Ti^{4+} nanotubes with different concentrations of Eu^{3+} (X=1.0, 2.0, 3.0, 4.0, 5.0 and 6.0 mol%).

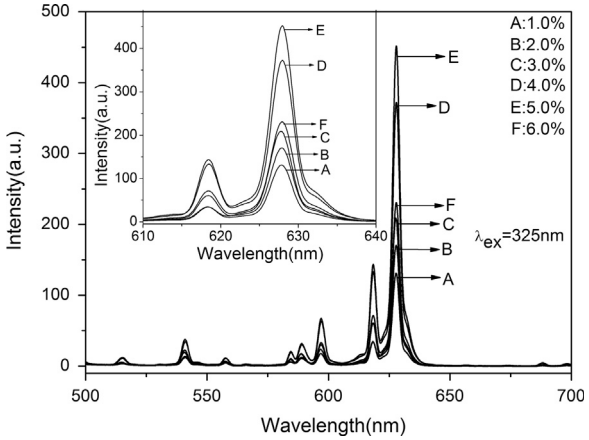

Fig. 4. The emission spectra of $Y_2O_2S:Eu^{3+}$, Mg^{2+}, Ti^{4+} nanotubes with different concentrations of Eu^{3+} ($X=1.0$, 2.0, 3.0, 4.0, 5.0 and 6.0 mol%) (the inset picture shows the enlarged emission spectra within 610–640 nm).

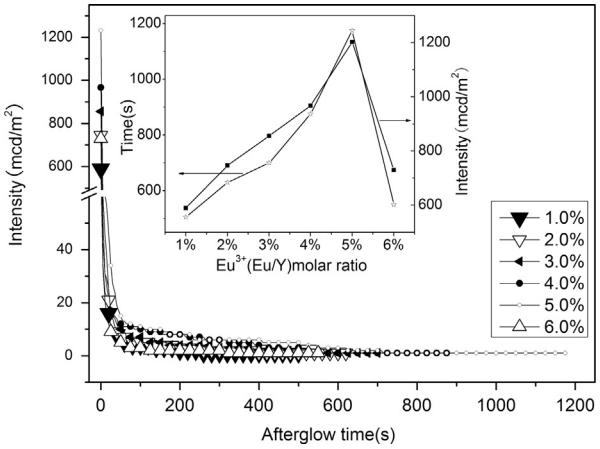

Fig. 5. The afterglow decay curves of phosphors with different concentrations of Eu^{3+} ($X=1.0$, 2.0, 3.0, 4.0, 5.0 and 6.0 mol%) (the inset picture shows the initial intensity and afterglow time of phosphors with different dopant contents).

maximum value. While dopant content is over 5.0 mol%, the intensity is decreased. The result may be explained as the following: in Y_2O_2S host, Eu^{3+} substitutes the site of Y^{3+}, and as the luminescence center. With the increase of Eu^{3+} content, the number of Eu^{3+} in the host keeps increasing, which leads to the increase of the intensity of spectra gradually. As the Eu^{3+} concentration further increase, there appears interaction between Eu^{3+} which are in the excited, and it may result in the production of mechanism of energy loss. The energy on an excited luminescence center can also be transferred to other luminescence centers if these luminescence centers are close enough so that they could be coupled together by some interaction. Due to the interaction, one of the two excited luminescence centers is forced to release energy and returns to ground state through non-radiative transition, and the other is inspired to a high excited state at the same time, which results in the decrease of luminescence transition probability. The excess of Eu^{3+} in the host could lead to the emerging of the concentration quenching which is the reason why the intensity of spectra decreased.

3.4. Afterglow decay curves and TL curves of samples

The afterglow decay curves of $Y_2O_2S:Eu^{3+}$, Mg^{2+}, Ti^{4+} nanotubes with different Eu^{3+} dopant contents ($X=1.0$, 2.0, 3.0, 4.0, 5.0 and 6.0 mol%) after irradiation with 365 nm UV light for 10 min are shown in Fig. 5. It is obvious that the phosphors release long-lasting phosphorescence. The nanotube phosphor shows a rapid decay at the beginning and the long-lasting phosphorescence further. However, the phosphor shows different afterglow properties with different dopant contents. The initial brightness and afterglow time of the phosphor show the tendency firstly increases then decreases gradually with dopant content. When dopant content is 5.0 mol%, the afterglow phosphor $Y_2O_2S:Eu^{3+}$, Mg^{2+}, Ti^{4+} nanotubes exhibits the highest initial brightness and the longest afterglow time, which are 1202 mcd/m^2 and 1175 s ($\geq$1 mcd/m^2), respectively. In comparison with the works of Liu et al. [20], in their works, the initial intensity and afterglow time of samples are lower than the results of the present work. The luminescence properties of our samples have an obvious improvement. Details are shown in Table 1. The reason is that the concentration of Eu^{3+} has a great influence on the luminescence properties of samples. When dopant content is 5.0 mol%, the afterglow phosphor shows optimal luminescence properties.

Table 1
The initial brightness and afterglow time of the phosphors.

The phosphors	Initial brightness (mcd/m^2)	Afterglow time (s) ($\geq$1 mcd/m^2)
Liu et al. [20]	960	450
The results of the present work	1202	1175

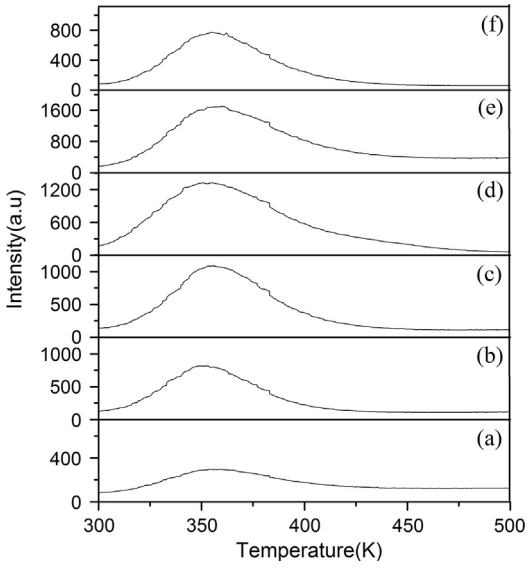

Fig. 6. The TL curves of phosphors $Y_2O_2S:Eu^{3+}$, Mg^{2+}, Ti^{4+} nanotubes with different dopant contents: (a) 1.0 mol%; (b) 2.0 mol%; (c) 3.0 mol%; (d) 4.0 mol%; (e) 5.0 mol%; (f) 6.0 mol%.

Table 2
E values of the samples with different concentrations of Eu^{3+}.

Concentration of Eu^{3+}-doped (mol%)	T_m (K)	T_1 (K)	T_2 (K)	τ (K)	δ (K)	ω (K)	μ_g	E (eV)
1.0	354	323	415	31	61	92	0.66	0.62
2.0	357	331	398	26	41	67	0.62	0.74
3.0	353	328	383	25	30	55	0.55	0.75
4.0	354	330	387	24	33	57	0.58	0.76
5.0	355	333	389	22	34	56	0.61	0.88
6.0	354	324	385	30	31	61	0.51	0.72

The afterglow mechanisms can be explained by the contribution from the electron traps formed by the co-doped Mg^{2+} and Ti^{4+} ions. The Mg^{2+} and Ti^{4+} occupy the same lattice sites as Y^{3+} ions do. To keep charge balance, 2 Y^{3+} ions are replaced by 1 Mg^{2+} and 1 Ti^{4+} ions. However, such replacement breaks the charge balance around local lattice site and causes the formation of new electronic donating and accepting levels between the host lattice band gap, that is, an excessive positive charge which serves as the electron trap around the doped Ti^{4+} ion is created. One of the ions absorbs energy and thermally transfers the excited electrons to another ion which serves as trap centers. The trap of stored energy which is constituted by Mg^{2+} and Ti^{4+} ions serves as the donor leveling, and Eu^{3+} serves as the acceptor leveling. The trapping of excited electrons and thermally released processes cause the appearance of afterglow [24].

TL spectrum is an important tool to investigate the luminous properties of phosphor. The afterglow luminance and time are found to depend strongly on the depth and the density of traps [25,26]. Fig. 6 represents the TL curves of samples with different concentrations of Eu^{3+} after irradiation with 365 nm UV radiation for 10 min. For all the samples, the TL peaks are located in the region of 323–383 K which are helpful to produce a longer duration of afterglow. In Fig. 6, all peaks are located in this region. With the increase of dopant content, the intensity of TL peak is increased gradually. And when the concentration of Eu^{3+} ions is 5.0 mol%, the intensity of TL peak reaches maximum, implying that moderate content of Eu^{3+} dopant can improve the trap density. But when dopant content exceeds 5.0 mol%, the intensity of TL peak begins to decrease because concentration quenching occurs [27].

The depth of traps in the samples can be estimated by analyzing the TL peak using equations given by Chen[28]:

$$E = c_\tau k T_m^2/\tau - b_\tau 2kT_m \quad (1)$$

$$c_\tau = 1.51 + 3(\mu_g - 0.42), \quad b_\tau = 1.58 + 4.2(\mu_g - 0.42) \quad (2)$$

$$\tau = T_m - T_1, \quad \delta = T_2 - T_m, \quad \omega = T_2 - T_1, \quad \mu_g = \delta/\omega \quad (3)$$

where T_m is the peak temperature, T_1 and T_2 are the low and high temperatures corresponding to the half peak intensity, δ is the right half width, ω is the total half intensity width, k is Boltzmann's constant, μ_g is the symmetry factor. The trap parameters are calculated using Eqs. (1)–(3) and listed in Table 2.

In order to produce long phosphorescence, the trapping levels need to locate at a suitable depth. If the trap level is too shallow, only small amount of electrons can be captured to traps. Under the action of thermal disturbances, electrons are easily released from traps and then combined with holes in the ground state, which results in shorter afterglow time. On the other hand, if the trap level is too deep, it is hard to return electrons to the excited state levels at room temperature, which also results in poor afterglow property. The sample doped with 5 mol% Eu^{3+} has the maximum intensity of TL peak and the deepest trap depth with 0.88 eV, and it shows the optimal initial luminance and afterglow time. From Fig. 6 and Table 1, for the Y_2O_2S:Eu^{3+}, Mg^{2+}, Ti^{4+} phosphor, the high trap density and deep trap depth is suitable to produce optimal afterglow properties.

4. Conclusions

Red long-lasting phosphor Y_2O_2S:Eu^{3+}, Mg^{2+}, Ti^{4+} nanotubes with different concentrations of Eu^{3+} are prepared through the hydrothermal method combining with a post-calcining process. Pure phase of $Y(OH)_3$ and Y_2O_2S can be obtained during the experiment. The morphology of the Y_2O_2S:Eu^{3+}, Mg^{2+}, Ti^{4+} phosphors inherits the tube-like shape from the precursors after calcinating for 6 h at 750 °C in CS_2 atmosphere. The Y_2O_2S:Eu^{3+}, Mg^{2+}, Ti^{4+} nanotubes have strong red-emission lines at 625 nm which ascribes to the transition from $^5D_0$ to $^7F_2$ level of Eu^{3+} ion under the 325 nm UV irradiation. While the sample doped with 5.0 mol% Eu^{3+} has the highest trap density and the deepest trap depth, which leads to the optimal initial luminance and afterglow time. Therefore, for red long-lasting phosphor Y_2O_2S:Eu^{3+}, Mg^{2+}, Ti^{4+} nanotubes, the optimal concentration of Eu^{3+} is 5.0 mol%.

Acknowledgments

This present work was financially supported by the National Natural Science Foundation of China (No. 51072128), Key Research Project of Science and Technology of Shanxi (No. 20110321040-01) and Program for the Top Young Academic Leaders of Higher Learning Institutions of Shanxi.

References

[1] S.Y. Kaya, E. Karacaoglu, B. Karasu, Effect of Al/Sr ratio on the luminescence properties of $SrAl_2O_4$:Eu^{2+}, Dy^{3+} phosphors, Ceramics International 38 (2012) 3701–3706.

[2] M. Bockrath, W.J. Liang, D. Bozovic, J.H. Hafner, C.M. Lieber, M. Tinkham, H. Park, Modulated chemical doping of individual carbon nanotubes, Science 291 (2001) 283–285.
[3] J.Y. Kuang, Y.L. Liu, J.X. Zhang, White-light-emitting long-lasting phosphorescence in Dy^{3+}-doped $SrSiO_3$, Journal of Solid State Chemistry 179 (2006) 266–269.
[4] L.X. Wang, L. Zhang, Y.D. Huang, D.Z. Jia, J.J. Lu, Effects of Gd^{3+} and Lu^{3+} co-doping on the long afterglow properties of yellowish-orange phosphor Y_2O_2S:Ti^{4+}, Mg^{2+}, Journal of Luminescence 129 (2009) 1032–1035.
[5] X. Wang, J. Zhang, Q. Peng, Y.D. Li, A general strategy for nanocrystal synthesis, Nature 437 (2005) 121–124.
[6] Y. Murazaki, K. Arak, K. Ichinomiya, A new long persistence red phosphor, Journal of Rare Earth Japan 35 (1999) 41.
[7] S.P. Mao, Q. Liu, M. Gu, D.L. Mao, C.K. Chang, Long lasting phosphorescence of Gd_2O_2S:Eu, Ti, Mg nanorods via a hydrothermal routine, Journal of Alloys and Compounds 465 (2008) 367–374.
[8] C.E. Cui, X. Lei, P. Huang, L. Wang, F. Yang, Influence of sulfuretted temperature on the luminescent properties of Y_2O_2S:Eu^{3+}, Mg^{2+}, Ti^{4+} nanoarrays, Journal of Luminescence 138 (2013) 138–142.
[9] A. Medina, L. Béjar, S.E. Borjas, J. Zarate, R. Vargas, G. Herrera, A. Ruiz, Characterization of ZnO nanoparticles with short-bar shape produced by chemical precipitation, Materials Letters 71 (2012) 81–83.
[10] E.Y. Bang, Daniel R. Mumm, Hye Ryoung Park, Myoung Youp Song, Lithium nickel cobalt oxides synthesized from Li_2CO_3, NiO and Co_3O_4 by the solid-state reaction method, Ceramics International 38 (2012) 3635–3641.
[11] A. Dikhtiarenko, S.A. Khainakov, J.R. García, J. Gimeno, I. de Pedro, J.Rodríguez Fernández, J.A. Blanco, Hydrothermal synthesis and physicochemical properties of ruthenium(0) nanoparticles, Journal of Alloys and Compounds 536 (2012) S437–S440.
[12] X. Wang, Y.D. Li, Synthesis and characterization of lanthanide hydroxide single-crystal nanowires, Angewandte Chemie International Edition 41 (2002) 4790.
[13] X. Wang, X.M. Sun, D.P. Yu, B.S. Zou, Y.D. Li, Rare earth compound nanotubes, Advanced Materials 15 (2003) 1442–1445.
[14] G. Jia, K. Liu, Y.H. Zheng, Y.H. Song, M. Yang, H.P. You, Highly uniform $Gd(OH)_3$ and Gd_2O_3:Eu^{3+} nanotubes: facile synthesis and luminescence properties, Journal of Physical Chemistry C 113 (2009) 6050–6055.
[15] Y.B. Mao, J.Y. Huang, R. Ostroumov, K.L. Wang, J.P. Chang, Synthesis and luminescence properties of erbium-doped Y_2O_3 nanotubes, Journal of Physical Chemistry C 112 (2008) 2278.
[16] Y.Z. Huang, L. Chen, L.M. Wu, Crystalline nanowires of Ln_2O_2S, $Ln_2O_2S_2$, LnS_2 (Ln=La, Nd), and La_2O_2S:Eu^{3+}. Conversions via the boron–sulfur method that preserve shape, Crystal Growth and Design 8 (2008) 739.
[17] L.Y. Yang, J.X. Wang, X.T. Dong, G.X. Liu, W.S. Yu, Synthesis of Y_2O_2S:Eu^{3+} luminescent nanobelts via electrospinning combined with sulfurization technique, Journal of Materials Science 48 (2013) 644–650.
[18] L.X. Yu, F.H. Li, H. Liu, Fabrication and photoluminescent characteristics of one-dimensional La_2O_2S:Eu^{3+} nanocrystals, Journal of Rare Earths 31 (2013) 356–359.
[19] J. Huang, Y.H. Song, Y. Sheng, K.Y. Zheng, H.B. Li, H.G. Zhang, Q. S. Huo, X.C. Xu, H.F. Zou, Gd_2O_2S:Eu^{3+} and Gd_2O_2S:Eu^{3+}/Gd_2O_2S hollow microspheres: solvothermal preparation and luminescence properties, Journal of Alloys and Compounds 532 (2012) 34–40.
[20] D. Liu, P. Huang, C.E. Cui, L.Wang, G.W. Jiang, Effects of simultaneous change of Mg^{2+} and Ti^{4+} contents on the luminescence properties of Y_2O_2S:Eu^{3+}, Mg^{2+}, Ti^{4+} nanotubes, Ceramics International (in press), http://dx.doi.org/10.1016/j.ceramint.2013.05.111, <http://www.sciencedirect.com/science/article/pii/S0272884213006275>.
[21] W.Y. Li, Y.L. Liu, P.F. Ai, Synthesis and luminescence properties of red long-lasting phosphor Y_2O_2S:Eu^{3+}, Mg^{2+}, Ti^{4+} nanopartiticles, Materials Chemistry and Physics 119 (2010) 52.
[22] H.H. Zeng, X.M. Zhou, L. Zhang, X.P. Dong, Synthesis and luminescence properties of a novel red long lasting phosphor Y_2O_2S:Eu^{3+}, Si^{4+}, Zn^{2+}, Journal of Alloys and Compounds 460 (2008) 704–707.
[23] S.Q. Deng, Z.P. Xie, Y.L. Liu, B.F. Lei, Y. Xiao, M.T. Zhen, Synthesis and characterization of Y_2O_2S:Eu^{3+}, Mg^{2+},Ti^{4+} hollow nanospheres via a template-free route, Journal of Alloys and Compounds 542 (2012) 207–212.
[24] P. Huang, F. Yang, C.E. Cui, L. Wang, X. Lei, Luminescence improvement of Y_2O_2S:Tb^{3+}, Sr^{2+}, Zr^{4+} white-light long-lasting phosphor via Eu^{3+} addition, Ceramics International 39 (2013) 5615–5621.
[25] T. Aitasalo, P. Deren, J. Holsa, H. Jungner, J.C. Krupa, M. Lastusaari, J. Legendziewicz, J. Niittykoski, W. Strek, Persistent luminescence phenomena in materials doped with rare earth ions, Journal of Solid State Chemistry 171 (2003) 114–122.
[26] L. Jing, C.K. Chang, D.L. Mao, B. Zhang, A new long persistent blue-emitting $Sr_2ZnSi_2O_7$:Eu^{2+},Dy^{3+} prepared by sol–gel method, Materials Letters 58 (2004) 1825–1829.
[27] S.W.S. Mckeever, Thermoluminescence of Solids, Cambridge University Press, New York150–151.
[28] R. Chen, Glow curves with general order kinetics, Journal of Electrochemical Society: Solid State Science 116 (1969) 1254–1257.